Effect of Strain Reversal on the Dynamic Spheroidization of Ti-6Al-4V during Hot Deformation

R.M. POTHS, G. ANGELLA, B.P. WYNNE, W.M. RAINFORTH, S.L. SEMIATIN, and J.H. BEYNON

The effect of strain-path reversal on the kinetics of dynamic spheroidization during subtransus hot working was determined for Ti-6Al-4V with a colony α structure. Isothermal torsion tests were conducted at a temperature of 815 °C and a strain rate of 0.001 s^{-1}; strain-path reversals were achieved by applying forward and reverse torsion sequentially. The kinetics of spheroidization were measured as a function of the local (macroscopic) strain for monotonic-deformation, reversed-torsion, and double-reversed-torsion tests. Strain-path reversal led to a reduction in the spheroidization kinetics compared with monotonic deformation for a given total strain. The slower rate of dynamic spheroidization associated with strain-path reversals was ascribed to a reduced rate of sub-boundary formation/lower sub-boundary energies, which drive the boundary splitting process, and less sharp α/β interface curvatures, which control the coarsening process that also contributes to spheroidization.

I. INTRODUCTION

INGOTS of conventional α/β titanium alloys, such as Ti-6Al-4V (Ti-6-4), are often processed commercially *via* a number of steps in order to refine the as-cast microstructure and to achieve the desired final product dimensions. Initially, hot working (and annealing) of ingot-cast material is performed in the β-phase field to produce a more uniform and finer structure. Upon cooling from the β field into the $\alpha + \beta$ phase field, the microstructure transforms; the morphology of the resulting structure is a function of the cooling rate. High cooling rates lead to Widmanstätten or martensitic structures, whereas slower cooling rates, prevalent in large billet products, result in colony or basketweave structures.[1] Subsequent hot working in the $\alpha + \beta$ phase field breaks down this microstructure, contributing to the formation of the more desirable equiaxed-α microstructure. This process, commonly referred to as globularization or spheroidization, can occur dynamically or statically during post deformation annealing. The equiaxed-α phase morphology gives several property benefits over a lamellar structure, including increased low-temperature ductility and improved fatigue-crack-initiation resistance.[2]

Due to the importance of spheroidization during the industrial processing of $\alpha + \beta$ titanium alloys, considerable work has been performed to investigate the kinetics and mechanisms of spheroidization. Dynamic spheroidization has been studied by several authors, including Seshacharyulu *et al.*,[3] Semiatin and co-workers,[4,5,6] and Korshunov *et al.*[7] For example, the work of Semiatin *et al.*[5] quantified the effect of deformation temperature on the dynamic spheroidization kinetics of Ti-6-4 at three strain rates. For a material with a prior-β grain size of 100 μm, they showed that the kinetics exhibit little dependence on temperature at a low strain rate (0.001 s^{-1}), but the rate of spheroidization decreases somewhat with increasing temperature at higher strain rates. The kinetics and mechanisms of *static* spheroidization (*i.e.,* those during post deformation annealing) have also been investigated by several authors, for example, Weiss *et al.*[2] and Stefansson *et al.*[8] Weiss *et al.*[2] proposed a two-stage mechanism for the spheroidization of α lamellae during deformation and annealing: lateral interfaces form within the α lamellae as a result of the formation of shear bands (due to localized shearing) or subgrain boundaries. The laths are subsequently broken up by interface-tension-driven β-phase penetration (*i.e.,* boundary splitting/grooving) along the sub-boundaries/shear bands, thus resulting in an equiaxed-α morphology. This mechanism is generally accepted and has been compared to the mechanism of geometric dynamic recrystallization observed in aluminum.[9] Recently, however, Stefansson *et al.*[8,10] have provided a more quantitative insight into static spheroidization kinetics and those processes which control static spheroidization. For example, it was shown that the grooving process accounts for only a moderate fraction of static spheroidization. The majority of the spheroidization occurs as a result of coarsening processes such as Ostwald ripening and termination migration.

Finite-element modeling has shown[11] that even simple industrial forming processes involve a number of strain-path changes. These can affect flow behavior, texture, and microstructure development in a number of materials. For example, the effects of deformation mode and strain path on the dynamic spheroidization kinetics of the titanium-based VT9 alloy were studied by Korshunov *et al.*[7] This work showed that different monotonic deformation modes, such as tension or torsion, result in similar spheroidization kinetics, but that large strain-path changes, such as that in reversed torsion testing, retard the spheroidization kinetics compared with monotonic deformation. These results are similar to those seen in work examining the effect of strain-path reversal

R.M. POTHS, Research Associate, B.P. WYNNE, Lecturer, and W.M. RAINFORTH and J.H. BEYNON, Professors, are with IMMPETUS, Department of Engineering Materials, The University of Sheffield, Sheffield, S1 3JD, United Kingdom. Contact e-mail: r.m.poths@sheffield.ac.uk G. ANGELLA, Scientific Researcher, is with the I.EN.I. Institute, Consiglio Nazionale delle Ricerche. Milano, Italy. S.L. SEMIATIN, Senior Scientist, Materials Processing/Processing Science, is with the Air Force Research Laboratory, Material and Manufacturing Directorate, AFRL/MLLM, Wright-Patterson Air Force Base, OH 45433-7817.

Manuscript submitted July 10, 2003.

on the dynamic recrystallization kinetics of stainless steel,[12] microalloyed steel,[13] and lead.[14] Similarly, the effect of strain-path changes on the flow-softening behavior of Ti-6-4 with a colony α microstructure was determined using a combination of hot rolling and axisymmetric compression testing by Semiatin *et al.*[15] Typical monotonic-deformation flow curves for such structures exhibited large peak stresses followed by significant flow softening; their results showed that a strain-path change after a prestrain greater than 0.2 resulted in lower peak stresses and only weak flow softening up to total strains of 1.2.

It can be concluded from the limited reported work that strain-path changes during the subtransus hot working of α/β titanium alloys affect both flow behavior and microstructural development. The present research was undertaken to quantify the dynamic spheroidization kinetics of a colony-α structure subjected to strain-path reversals and to relate the observed differences to the microstructure-evolution mechanisms.

II. MATERIAL AND EXPERIMENTAL PROCEDURES

A. *Material*

The material used in this work was a commercially produced α/β titanium alloy, Ti-6Al-4V (Ti-6-4). The material was received as a hot-rolled, 30-mm-diameter bar, which had been mill annealed at 700 °C for 2 hours, resulting in a microstructure comprising equiaxed-α and transformed β. This alloy has a nominal β-transus temperature of 995 °C. Its composition (in wt pct) was determined to be 6.6 aluminum, 4.1 vanadium, 0.2 oxygen, 0.06 carbon, 0.07 nitrogen, and 0.004 hydrogen, the balance being titanium.

In order to produce a microstructure similar to that used in previous work,[5] a multiple-stage heat treatment was carried out immediately prior to mechanical testing. This treatment consisted of 815 °C/6 min + 1040 °C/1 min + 950 °C/2 min + 815 °C/10 min, the final temperature being the test temperature; for each temperature change, a heating rate of 490 °C/min was used. The microstructure at the test temperature (determined on water-quenched samples) consisted of equiaxed prior-β grains containing a transformed structure of colony α. The prior-β grain size was ~110 μm, the mean α-lamella thickness was ~1 μm, and the prior-β grain boundaries were decorated with a 2-μm-thick layer of α phase. Figure 1 shows a backscattered electron (BSE) image of this microstructure acquired in a scanning electron microscope (SEM) from a polished but unetched surface. The contrast in BSE images of this microstructure is due to differences in the composition of the α and β phases, which leads to Z contrast; hence, α is the darker phase and β is the lighter phase. Additionally, channelling contrast is also present, predominantly in the α phase, and reflects local crystal orientation. However, this contrast is weaker than the Z contrast.

Bulk texture analysis was performed on the heat-treated-and-quenched material using an X-ray diffraction technique. Partial pole figures were used in conjunction with popLA,[16] the preferred orientation package from Los Alamos, to compute sample-orientation distributions and complete pole figures. The texture was found to be relatively weak. For example, the (0002) α-phase pole figure (Figure 2) revealed a weak basal-fiber-texture component.

FIGURES

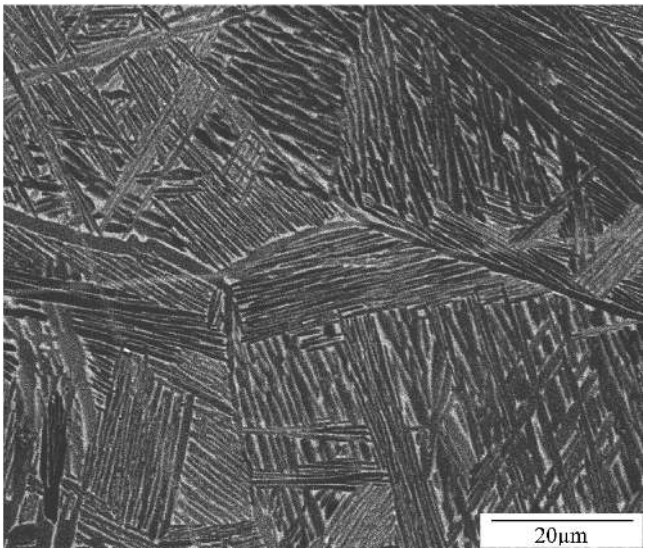

Fig. 1—BSE image of the colony-α microstructure developed by heat treatment followed by water quenching.

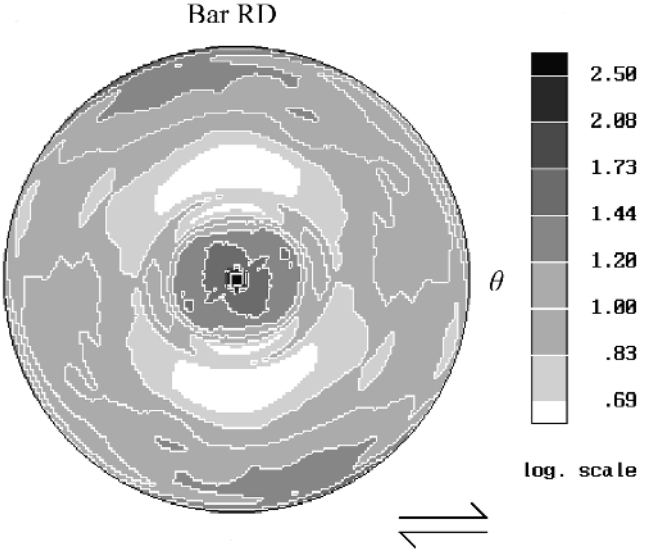

Fig. 2—α-phase (0002) pole figure of the heat-treated-and-water-quenched material. The rolling direction of the initial material (bar) and shear direction of the torsion tests are indicated.

B. *Torsion-Testing Procedures*

To assess the effect of strain-path reversal on the dynamic globularization kinetics, isothermal forward/reverse torsion tests were conducted using the torsion component of the special-purpose arbitrary strain-path rig at the University of Sheffield (United Kingdom).[17] The torsion portion of this system includes a 15 kW a.c. motor and an ACS 600 frequency controller. The motor has a continuously variable speed range of ±1450 rpm. The sample is held in three-jaw chucks and is heated by a 15 kW induction heater. The sample and air-cooled chucks are separated by copper baffles. The application of torsion deformation is controlled by a pneumatic

clutch/brake system to avoid transient deformation during motor reversal. Rapid sample cooling is achieved by a water-quench system. The torque is recorded using a half Wheatstone-bridge strain-gage system fitted with a strain gage amplifier, and the angular rotation is measured by a rotary encoder.

In the present work, solid torsion samples were machined to a gage diameter of 6.6 mm and length of 13.2 mm, with a thermocouple inserted offset from the deformation zone. Prior to testing, samples were heated using the aforementioned schedule. Tests were carried out using strictly forward torsional straining to impose monotonic deformation or using sequential forward and reversed torsion to achieve complete strain-path reversals. In either case, samples were deformed at a surface effective strain rate of 0.001 s^{-1} to surface effective strains of either 2 or 3 (Figure 3). Both strain and strain rate vary across the diameter of solid torsion specimens.[18] The linear increase in strain from the sample center to the surface allows a range of strains to be studied in each sample. In this way, the relationship between the applied strain and fraction spheroidized over a large range of strains was assessed using a limited number of tests.

Previous work[5] for deformation at 815 °C has shown that the strains for initiation and completion of dynamic spheroidization vary little when the strain rate is increased from 0.001 to 10 s^{-1}. To confirm that the radial variation in strain rate inherent in torsion specimens also led to little change in the values of these critical strains, additional monotonic tests were conducted at a surface strain rate of 0.0018 s^{-1} in order to impose a strain rate of 0.001 s^{-1} at the radial position having a strain of ~1. This value was chosen to correspond to the strain resulting in 50 pct spheroidization after monotonic deformation at a nominal strain rate of 0.001 s^{-1}.

Effective stress-strain curves were calculated from the twist-torque data recorded during testing using standard equations.

C. *Microstructure Evaluation*

Deformed-and-quenched microstructures were examined on axial cross sections of the torsion samples using BSE imaging in a JEOL* 6400 SEM. The monotonic samples were also examined on tangential planes corresponding to local effective strains of ~1 and ~1.4, to establish the influence of the plane of sectioning (relative to the deformation direction) on the measured spheroidization kinetics. Two different strain metrics were used in the analysis of microstructure evolution. The first comprised the total effective strain, or simply total strain, in which the absolute values of the strains were summed. For the second strain measure, denoted as "net" strain, the sign of the strain was taken into account. Hence, a deformation characterized by a forward strain of 1 and a reverse strain of 1 would yield a total strain of 2, whereas the net strain would be zero.

The volume fractions of spheroidized microstructure were measured using a point-counting method. For this purpose, a series of digital BSE images were obtained at positions across the diameter of each axial section. For the monotonic samples (sample M), these positions corresponded to increments in local strain of ~0.3; in the reverse and double-reverse samples (samples R and DR, respectively), images were taken at three positions, corresponding to local total strains of 0.73, 1.29, and 1.57 (sample R) or 1.16, 2.04, and 2.49 (sample DR). These images were then processed to improve the contrast between the α and β phases before a 96-point grid (point spacing of 5 μm) was positioned over the image. The microstructure at each point was assessed in terms of the phase present and the morphology of each phase; α-phase constituents whose aspect ratio was less than or equal to approximately 2:1 were defined as spheroidized (Figure 4). A minimum of

*JEOL is a trademark of Japan Electron Optics Ltd., Tokyo.

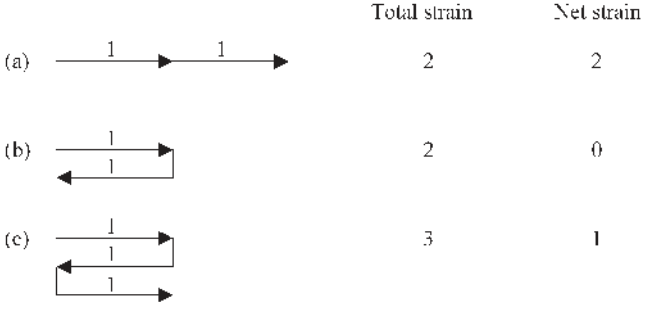

Fig. 3—Schematic illustration of the deformation paths used in the present work: (*a*) monotonic deformation (M), (*b*) reversed deformation (R), and (*c*) double-reversed deformation (DR).

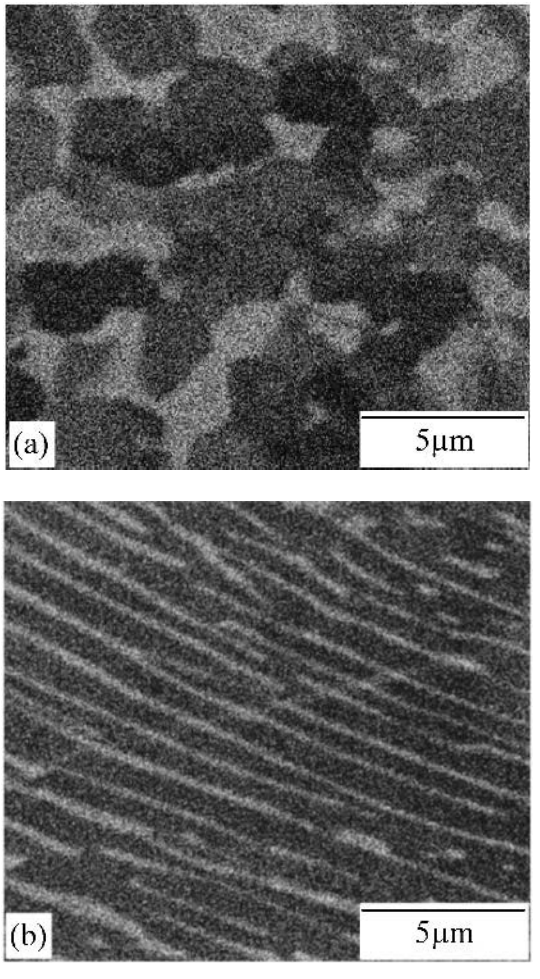

Fig. 4—SEM BSE micrographs illustrating examples of (*a*) spheroidized-α phase and (*b*) colony-α phase.

384 points (four image positions) was analyzed for each strain value examined.

III. RESULTS

The principal results of this work comprised the measured flow behavior, microstructure observations, and the determination of dynamic spheroidization kinetics.

A. *Flow Behavior*

Flow curves for monotonic torsion exhibited a peak flow stress at low strains (≤0.1) followed by significant flow softening before reaching almost steady-state flow at strains greater than 0.6 (Figure 5). The peak stress at the higher strain rate ($0.0018\ s^{-1}$) exceeded that at the lower strain ($0.001\ s^{-1}$) by ~10 MPa, but the strain at which steady state was achieved and the steady-state flow stress were similar. The steady-state comparison is more significant, inasmuch as the strain required for the *initiation* of dynamic spheroidization (discussed subsequently) was of the order of 1, which is well within the steady-state flow regime.

Strain reversal following forward torsion to a strain of 1 resulted in a *lower* flow stress upon reloading. However, difficulties associated with data retrieval prevented the accurate measurement of the reloading flow stress. Hence, further work is required before a more detailed description of this phenomenon can be provided.

B. *Microstructure Evolution*

Microstructure evolution during monotonic deformation at a temperature of 815 °C and a strain rate of $0.001\ s^{-1}$ (sample M) is summarized in Figure 6. At an effective strain of 0.39 (Figure 6(a)), a small amount of kinking of the lamellae had occurred, but no significant changes to the microstructure morphology were observed. After a strain of 1.01 (Figure 6(b)), some spheroidization and kinking of the α lamellae were noted. A significant increase in the level of spheroidization was observed with a further increase in strain to 1.35, with many of the remaining lamellae showing some degree of kinking (Figure 6(c)). In addition, at strains of 1.01 and 1.35, the two α morphologies (lamellar and spheroidized) were grouped in clusters apparently related to the original α colonies formed during the heat treatment. A strain of 1.63 resulted in an almost entirely spheroidized structure with only small areas of kinked lamellae remaining (Figure 6(d)). Similar microstructural features were observed in samples sectioned tangentially to the axis of rotation. An increase in the strain rate to $0.0018\ s^{-1}$ had little effect on the microstructure (observed in axial cross sections), with the lamellar kinking and spheroidized fraction showing a similar variation with strain.

The strain path for sample R, consisting of a forward torsional strain of 1 followed by a reversed torsional strain of 1 (*i.e.,* total strain of 2, and net strain of 0), resulted in a marked change in microstructure evolution. For this deformation, the number of kinked or spheroidized α lamellae at a given level of strain was significantly lower (Figure 7). As for the monotonic tests, the morphology of the α phase appeared to be similar within a colony, but varied from colony to colony, particularly at higher total strains (Figure 7(c)). The difference between the microstructures observed for increasing local strains was also less in sample R than that seen across the radius of sample M.

Figure 8 illustrates the effect of an additional *forward* torsional strain of 1 (sample DR, Figure 3) on the evolution of microstructure (total strain = 3, net strain = 1). At a given total level of strain, there is a small increase in the fraction spheroidized of α phase relative to that for sample R (Figure 7). A greater number of kinked α lamellae were observed also, although the kinking was less pronounced than that seen in sample M.

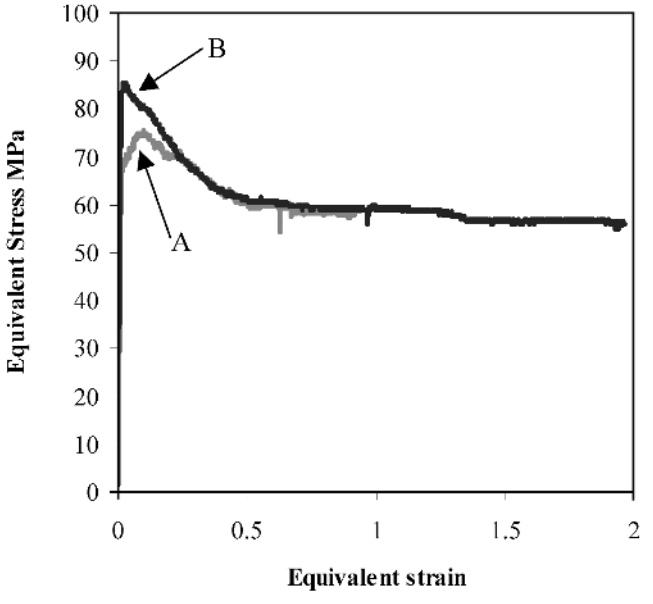

Fig. 5—Effective stress-strain curves for monotonic deformation illustrating the negligible effect of strain rate on the steady-state flow stress. A: surface effective strain rate of $0.001\ s^{-1}$, and B: surface effective strain rate of $0.0018\ s^{-1}$.

C. *Spheroidization Kinetics*

Measurements of the percent spheroidized *vs* strain following monotonic deformation at 815 °C and at a strain rate of $0.001\ s^{-1}$ are summarized in Figure 9. The strain for the initiation of spheroidization was ~0.4. Above this strain, the kinetics were somewhat rapid, with 95 pct spheroidization observed at a strain of ~1.5. The error bars in Figure 9 indicate the 95 pct confidence limits for the percent spheroidized and do not take into account errors in sample position measurements, which would affect the local value of strain; this issue is discussed further in Section IV. Furthermore, the results in Figure 9 for samples cut along a tangential plane show good agreement with those taken from axial cross sections. The kinetics of spheroidization during monotonic deformation at a strain rate of $0.0018\ s^{-1}$ were apparently more rapid than the kinetics measured for the slower strain rate at strains less than 1 (Figure 10). This suggests that there could be a strain-rate effect under these conditions, and this requires further investigation.

The effect of strain-path reversal on the kinetics of dynamic spheroidization is summarized in Figure 11, which is a comparison of the percent spheroidized α *vs* total local strain (closed symbols) and net local strain (open symbols) fol-

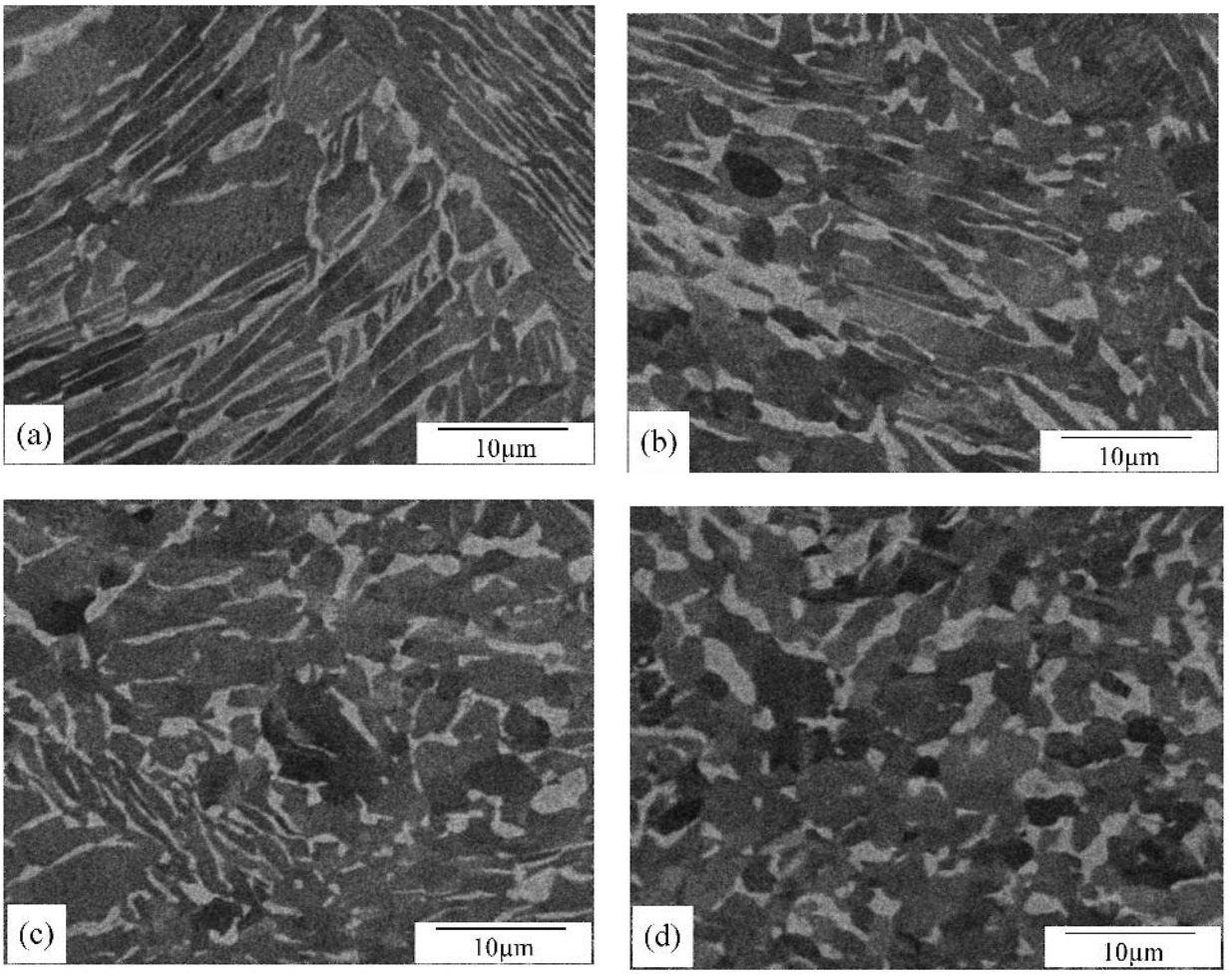

Fig. 6—SEM BSE micrographs illustrating dynamic spheroidization during monotonic deformation at 815 °C, 0.001 s^{-1}. Local strains and percent spheroidized were (*a*) 0.39, 0 pct; (*b*) 1.01, 21 pct; (*c*) 1.35, 65 pct; and (*d*) 1.63, 94 pct.

lowing monotonic (sample M), reversed (sample R), and double-reversed (sample DR) deformation. When plotted against the total local strain, the spheroidization rate for both the R and DR samples was retarded at strains around 1, compared to that for monotonic deformation. The plot of percent spheroidized α *vs* net strain indicated that total strain is a more meaningful parameter in studying the effect of strain path on dynamic spheroidization kinetics. The microstructure present at the end of the initial forward strain is, essentially, the starting microstructure for further monotonic deformation and strain-path tests. Thus, comparison of these data and those from the final microstructures allows the effect of monotonic and reversed strains on the dynamic spheroidization kinetics to be quantified. After a low initial forward strain (0.39), no spheroidization had occurred; higher forward strains of 0.67 and 0.79 led to 7 and 11 pct spheroidization, respectively. A second forward strain resulted in increments in percent spheroidized of 62 and 77 pct for strain increments of 0.62 and 0.78 (to total strains of 1.29 and 1.57, respectively). Reversed straining after the forward deformation resulted in the same increase in total strain (*i.e.,* the same amount of work done), but not the same increase in the fraction spheroidized. Increases of just 25 and 31 pct spheroidized were observed following similar reversed-strain increments. After a further forward strain was applied, the rise in percent spheroidized was not considerable. In fact, increases in total local strain of 0.43, 0.75, and 0.92 (to total strains of 1.16, 2.04, and 2.49, respectively) led to increments in spheroidization of just 10, 18, and 19 pct, respectively.

IV. DISCUSSION

A. *Effect of Strain Path on Spheroidization Kinetics*

The effect of strain path on dynamic spheroidization kinetics was interpreted for both monotonic and reversed types of deformation. With regard to monotonic deformation, the dynamic spheroidization kinetics from the present torsion tests (Figure 9) can be compared with previous measurements[5] conducted on material with a similar initial microstructure, but deformed in axisymmetric compression (Figure 12). In both cases, the nominal strain rate was 0.001 s^{-1}, and the deformation temperature was 815 °C. The data show reasonable agreement, although the strains for the initiation and completion of spheroidization are slightly *greater* for compression than for torsion. The rate of spheroidization in compression is also slightly lower due to the greater amount of strain required for completion of spheroidization. From a quantitative

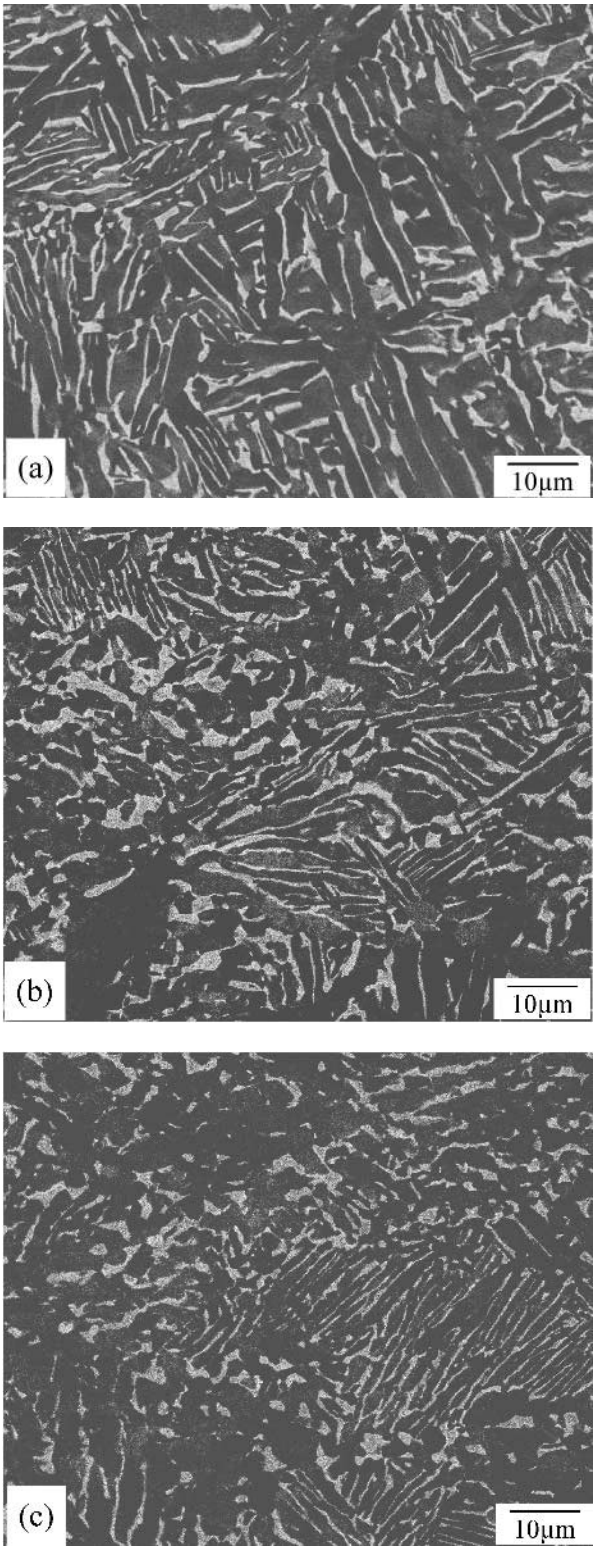

Fig. 7—SEM BSE micrographs illustrating dynamic spheroidization during reversed deformation at 815 °C, 0.001 s^{-1} following a forward strain of 1. Local *total* strains and percent spheroidized were (*a*) 0.73, 13 pct; (*b*) 1.29, 32 pct; and (*c*) 1.57, 42 pct.

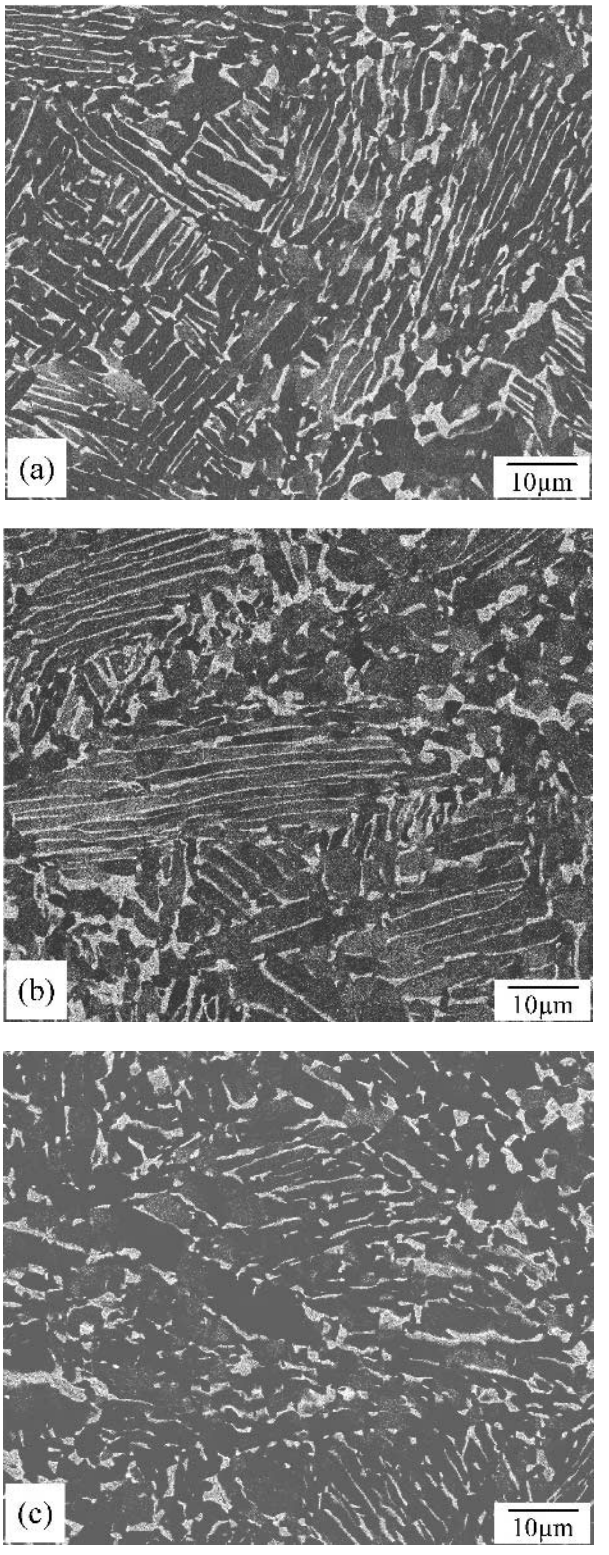

Fig. 8—SEM BSE micrographs illustrating dynamic spheroidization during double-reversed deformation at 815 °C, 0.001 s^{-1} with two prior strains of 1 in reverse directions. Local *total* strains and percent spheroidized were (*a*) 1.16, 23 pct; (*b*) 2.04, 50 pct; and (*c*) 2.49, 61 pct.

standpoint, spheroidization was first observed at a strain of ~0.4 and was 95 pct complete by a strain of ~1.5 for the present torsion tests. In contrast, spheroidization during compression testing initiated at a strain of ~0.7 and was almost complete at a strain of ~2.6. It is possible that this difference is due to the method used to assess the progress of spheroidization.

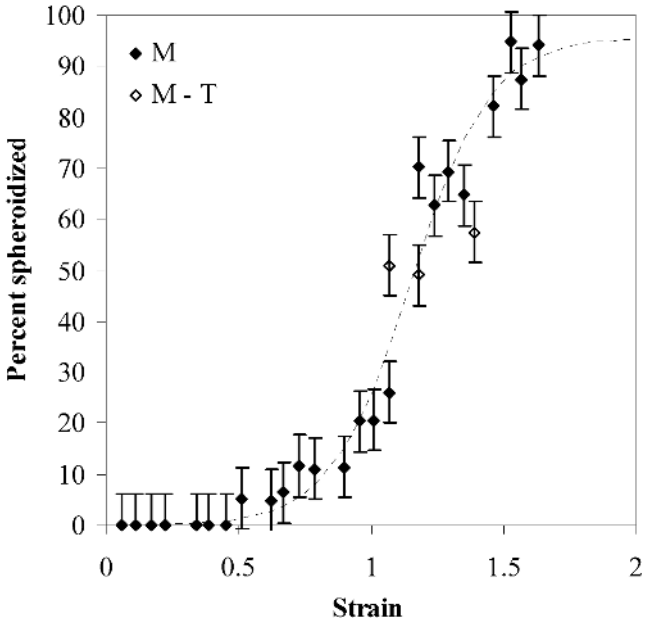

Fig. 9—Percent spheroidized α *vs* local effective strain for monotonic deformation determined from axial cross sections (M) or tangential sections (M-T).

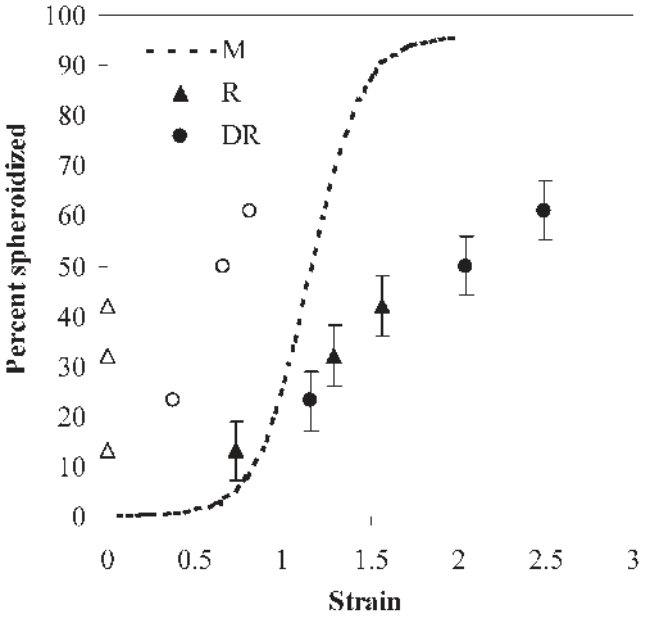

Fig. 11—Percent spheroidized α *vs* local strain for monotonic (M), reversed-torsion (R), and double-reversed torsion (DR) deformation paths. Closed data points denote total strain, and open data points denote net strain.

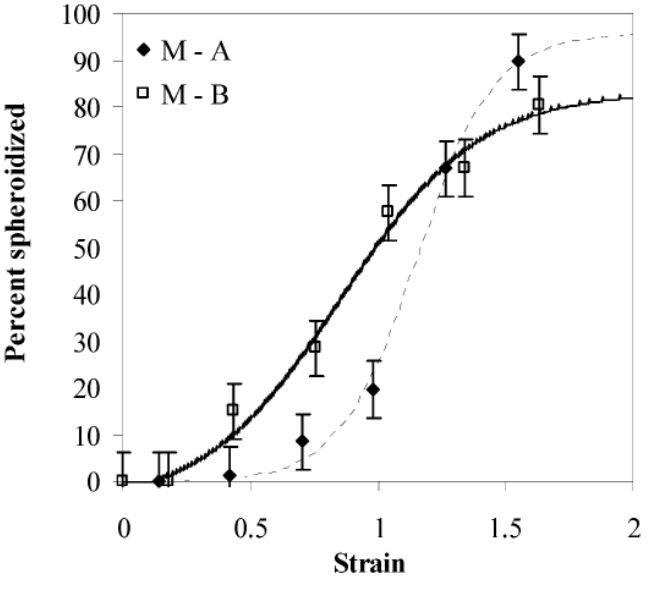

Fig. 10—Percent spheroidized α *vs* local effective strain for monotonic deformation at a surface effective strain rate of 0.001 s^{-1} (M-A) or 0.0018 s^{-1} (M-B).

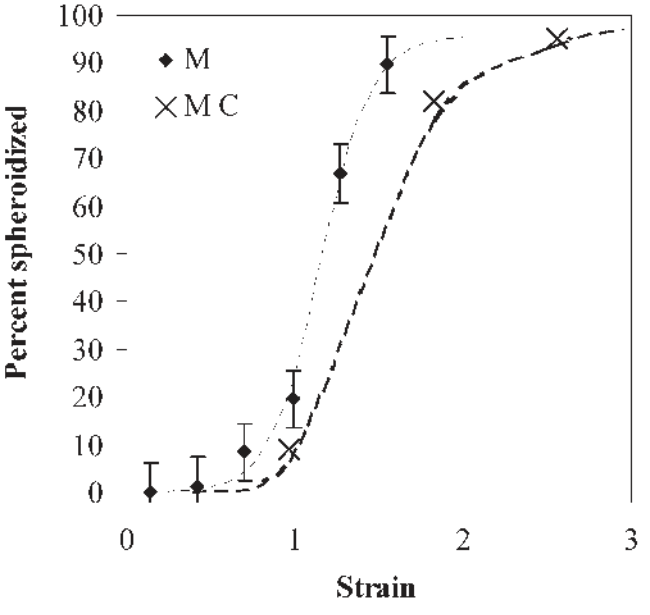

Fig. 12—Comparison of dynamic spheroidization kinetics for monotonic torsion (M, present work) and axisymmetric compression (MC, Ref. 5).

Semiatin *et al.*[5] used an image-analysis technique based on the *measured* aspect ratio to determine the morphology of the α phase, whereas the current research was based on a *qualitative* judgement of the aspect ratio. Also, the spheroidized α grains did not always clearly have a layer of β phase separating them (Figure 4(b)), although orientation contrast suggested that high-angle grain boundaries (rather than subgrain boundaries/shear bands) were separating them. The assumption that spheroidization was complete in such areas was made in performing all of the measurements presented in this work, thus making the comparison among the various strain paths internally consistent. Such an approach would be at variance with the compression data, however, for which a similar assumption was *not* made.

Another possible source of error in the data in Figures 9 through 11 is related to the measurement of the position at which the BSE images were obtained and, thus, the local strains associated with each microstructure. In torsion samples, the strain varies linearly across the diameter of the gage section, with a minimum (zero strain) at the center and a maximum at the surface.[19] An error of 100 μm in the position along a

radial line across the sample would lead to an error in the strain of ~0.06 (in a sample deformed to a total strain of 2). Such an error would be especially important for strains in the range between 1 and 1.5 (for monotonic deformation), because the rate of increase in the percent spheroidized with increasing strain is high in this region.

The data in Figure 11 highlight the major effect of strain reversal on the dynamic spheroidization kinetics of Ti-6Al-4V with a colony α microstructure. Compared with monotonic deformation, the kinetics were significantly retarded when the direction of the second strain was reversed. Applying a further forward strain after the strain reversal did not increase the kinetics; rather, a further retardation was observed. Indeed, the strain increment between the microstructures imaged in Figures 6(a) and (d) (sample M) was similar to that for the structures imaged in Figures 8(a) and (c) (sample DR), but the microstructural differences between the latter pair of micrographs were significantly less.

The present strain-path results can be compared with previous observations by Korshunov *et al.,*[7] who investigated the effect of strain reversal on dynamic spheroidization kinetics in alloy VT9 (Ti-6.6Al-3.5Mo-1.7Zr-0.27Si, in wt pct) (Figure 13). These former tests were conducted at a deformation temperature of 960 °C and strain rate of 0.001 s^{-1}. For the monotonic deformation modes, the rate of spheroidization was slightly higher (but within the reported 95 pct confidence limits) for samples deformed under torsion compared to that for samples deformed in tension, a result similar to that in the present work (Figure 12). The work of Korshunov *et al.* also revealed that forward torsion resulted in ~55 pct spheroidization at a strain of ~0.7, whereas a strain-path reversal at a strain of ~0.4 reduced the amount spheroidized to ~40 pct at a total strain of ~0.8. Further iterations of strain-path reversal after strain increments of 0.4 led to a drastic reduction in the rate of spheroidization with little increase in the percent spheroidized from a strain of ~0.8 to ~1.6. The greater reduction in the rate of spheroidization observed in the work of Korshunov *et al.,* compared to the current work, could be attributed to several factors, such as the smaller increments of strain applied between strain-path changes or differences in the starting thickness of the α lamellae. However, the general trend observed in the present and previous investigations is similar.

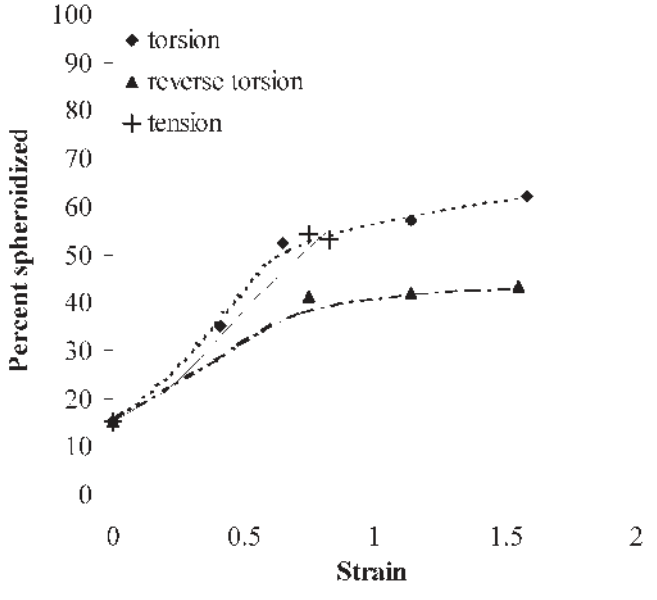

Fig. 13—Comparison of dynamic spheroidization kinetics of alloy VT9 deformed at 960 °C, 0.001 s^{-1} *via* uniaxial tension, torsion, or reversed torsion.[7]

B. *Dynamic Spheroidization Mechanisms*

Two factors appear to control the rate of dynamic spheroidization: the development of sub-boundaries within the α (and possibly β) lamellae and dynamic coarsening processes. With regard to the first of these factors, Weiss *et al.,*[2] Stefansson and Semiatin,[10] and Seshacharyulu *et al.*[20] have all suggested the importance of the formation of internal boundaries in the α phase as a precursor to boundary-splitting/grooving processes that contribute to spheroidization. The present results suggest that the work imposed during deformation is not being used effectively for spheroidization. That is to say, a strain-path reversal may result in a reduced rate of dislocation multiplication relative to that for a monotonic deformation, because of reduced interaction of dislocations with obstacles such as α/β interfaces. This would reduce the rate of recovery, which controls the rate at which sub-boundaries form. Furthermore, the misorientation across sub-boundaries formed during deformation involving a strain-path reversal would also be less, thus reducing the boundary energy and, hence, the grooving rate. The formation of shear bands and shear "offsets" due to slip transfer across the α-β boundaries[21] could also be retarded by the strain reversal.

A comparison of the thickness of the α lamellae prior to deformation (~1 μm) and the diameter of the spheroidized α particles (~2 to 4 μm) in the monotonic sample (Figure 6) also suggests that coarsening processes, such that reported by Semiatin and Stefansson[10] for static spheroidization, may play a role during dynamic spheroidization. The coarsening processes are driven by a reduction in surface energy *via* mass transport from regions of a small radius of curvature to regions of a high radius of curvature. Monotonic deformation would be expected to enhance coarsening through the development of α-phase segments with a small radii of curvature *via* platelet kinking and the development of slip steps due to slip transfer across α/β interfaces. On the other hand, the present work reveals that reversed deformation minimizes platelet kinking (*e.g.,* Figures 7 and 8) as well as the formation of shear bands and slip steps. Hence, the development of the α phase required to initiate coarsening processes is achieved in fewer locations, so a reduced rate of dynamic spheroidization would be expected during deformation involving a strain-path reversal, as was observed.

V. SUMMARY AND CONCLUSIONS

The effect of strain-path reversal on the dynamic spheroidization kinetics of the colony-α microstructure in α/β titanium alloys was established *via* torsion testing of Ti-6Al-4V at 815 °C and a strain rate of 0.001 s^{-1}, with reversals imposed after strain increments of 1. The following conclusions may be drawn from this work:

1. Strain-path reversal at strains greater than that required for the initiation of spheroidization results in a reduction in the kinetics of dynamic spheroidization compared with continuous (monotonic) deformation. A second reversal

of strain path appears to result in a yet further reduction in the dynamic spheroidization kinetics.

2. The reduction in kinetics due to strain-path reversal may be ascribed to a reduction in both boundary-splitting and coarsening processes, which appear to control dynamic spheroidization. Boundary splitting is retarded because of the slower rate of formation of sub-boundaries and the lower sub-boundary energy developed during deformations comprising strain-path changes. Strain-path reversal also appears to reduce the initiation of coarsening processes that lead to lower-aspect-ratio α lamellae, due to the reduction in α/β interface energy associated with the development of α-platelet kinking and slip steps across the α lamellae.
3. The present results highlight the difficulty of achieving a spheroidized microstructure for α/β titanium alloys *via* industrial hot-deformation processes which invariably involve strain-path changes. Thus, *static* spheroidization kinetics may play a very important role in the development of a uniform, fine microstructure for this class of alloys.

ACKNOWLEDGMENTS

The present work was supported by the Air Force Office of Scientific Research (AFOSR) and the AFOSR European Office of Aerospace Research and Development (AFOSR/EOARD) under Contract No. F61775-00-WE063. The encouragement of the AFOSR program managers (Drs. C.H. Ward and C.S. Hartley) is greatly appreciated.

REFERENCES

1. H.M. Flower: *Mater. Sci. Technol.,* 1990, vol. 6, pp. 1082-92.
2. I. Weiss, F.H. Froes, D. Eylon, and G.E. Welsch: *Metall. Trans. A,* 1986, vol. 17A, pp. 1935-47.
3. T. Seshacharyulu, S.C. Medeiros, W.G. Frazier, and Y.V.R.K. Prasad: *Mater. Sci. Eng. A,* 2002, vol. A325, pp. 112-25.
4. E.B. Shell and S.L. Semiatin: *Metall. Mater. Trans. A,* 1999, vol. 30A, pp. 3219-29.
5. S.L. Semiatin, V. Seetharaman, and I. Weiss: *Mater. Sci. Eng. A,* 1999, vol. A263, pp. 257-71.
6. S.L. Semiatin, J.F. Thomas, and P. Dadras: *Metall. Trans. A,* 1983, vol. 14A, pp. 2363-74.
7. A.A. Korshunov, F.U. Enikeev, M.I. Mazurskii, G.A. Salishchev, A.V. Muravlev, P.V. Chistyakov, and O.V. Dmitriev: *Russ. Metall.,* 1994, vol. 3, pp. 103-08.
8. N. Stefansson, S.L. Semiatin, and D. Eylon: *Metall. Mater. Trans. A,* 2002, vol. 33A, pp. 3527-34.
9. J.K. Solberg, H.J. McQueen, N. Ryum, and E. Nes: *Phils. Mag. A,* 1989, vol. 60, pp. 447-71.
10. N. Stefansson and S.L. Semiatin: *Metall. Mater. Trans. A,* 2003, vol. 34A, pp. 691-98.
11. J.H. Beynon: *Phils. Trans. R. Soc. London A,* 1999, vol. 357, pp. 1573-87.
12. G. Angella, B.P. Wynne, J.H. Beynon, and W.M. Rainforth: in *THERMEC '2000,* T. Chandra, ed., Elsevier Science Ltd., Oxford, United Kingdom, 2000, published on CD.
13. R. Bartolome, J.I. Astiazaran, A. Iza-Mendia, and I. Guitierrez: in *Thermomechanical Processing of Steels,* D.J. Naylor, ed., IOM Communications, London, United Kingdom, 2000, pp. 221-30.
14. X.J. Zhang, P.F. Thomson, and P.D. Hodgson: in *THERMEC'97,* T. Chandra and T. Sakai, eds., TMS, Warrendale, PA, 1997, pp. 1705-11.
15. S.L. Semiatin, J.O. Brown, T.M. Brown, D.P. DeLo, T.R. Bieler, and J.H. Beynon: *Metall. Mater. Trans. A,* 2001, vol. 32A, pp. 1556-59.
16. S.I. Wright and U.F. Kocks: *User's Manual for popLA,* Report LA-CC-89-18, Los Alamos National Laboratory, Los Alamos, NM, 1995.
17. G. Angella: Ph.D. Thesis, University of Sheffield, Sheffield, United Kingdom, 2002.
18. D.R. Barraclough, H.J. Whittaker, K.D. Nair, and C.M. Sellars: *JTEVA,* 1973, vol. 1, pp. 220-26.
19. U.F. Kocks, C.N. Tome, and H.-R. Wenk: *Texture and Anisotropy,* 1st ed., Cambridge University Press, Cambridge, United Kingdom, 1998.
20. T. Seshacharyulu, S.C. Medeiros, J.T. Morgan, J.C. Malas, W.G. Frazier, and Y. Prasad: *Scripta Mater.,* 1999, vol. 41, pp. 283-88.
21. S.L. Semiatin and T.R. Bieler: *Acta Mater.,* 2001, vol. 49, pp. 3565-73.